Journal of Materials Chemistry B

PAPER

View Article Online
View Journal

Cite this: DOI: 10.1039/c6tb00126b

A synergic nanoantioxidant based on covalently modified halloysite–trolox nanotubes with intra-lumen loaded quercetin†

Marina Massaro,[a] Serena Riela,*[a] Susanna Guernelli,[b] Filippo Parisi,[c] Giuseppe Lazzara,[c] Andrea Baschieri,[b] Luca Valgimigli[b] and Riccardo Amorati*[b]

Received 15th January 2016,
Accepted 26th February 2016

DOI: 10.1039/c6tb00126b

www.rsc.org/MaterialsB

We describe the preparation and properties of the first example of a synergic nanoantioxidant, obtained by different functionalizations of the external surface and the inner lumen of halloysite nanotubes (HNTs). Trolox, a mimic of natural α-tocopherol, was selectively grafted on the HNT external surface; while quercetin, a natural polyphenolic antioxidant, was loaded into the inner lumen to afford a bi-functional nanoantioxidant, HNT–Trolox/Que, which was investigated for its reactivity with transient peroxyl radicals and a persistent 1,1-diphenyl-2-picrylhydrazyl (DPPH•) radical in comparison with the corresponding mono-functional analogues HNT–Trolox and HNT/Que. Both HNT–Trolox and HNT/Que showed good antioxidant performance in the inhibited autoxidation of organic substrates; however HNT–Trolox/Que protection by reaction with peroxyl radicals was 35% higher in acetonitrile and 65% in chlorobenzene, as compared to the expected performance based on the sum of contributions of NHT-Trolox and NHT/Que. Similar enhancement was observed also in the trapping of DPPH• radicals. Synergism between the distinct antioxidant functions was based on the rapid reaction of externally exposed Trolox (rate constant with peroxyl radicals was 1.1×10^6 M^{-1} s^{-1} and 9×10^4 M^{-1} s^{-1} respectively in chlorobenzene and acetonitrile, at 30 °C), followed by its regeneration by quercetin released from the HNT lumen. The advantages of this novel nanoantioxidant are discussed.

Introduction

Oxidative degradation of organic materials, such as polymers, edible oils, foods and cosmetics, is due to a radical-chain mechanism, named as autoxidation or lipid peroxidation, in which alkyl radicals from the substrate are converted by atmospheric O_2 into peroxyl radicals (ROO•) that propagate the oxidative chain.[1] Chain-breaking antioxidants slow down the autoxidation rate by trapping ROO• radicals, as shown by eqn (1), and are mainly represented by (poly)phenols, aromatic amines and some conjugated organic acids, such as ascorbic acid.[2]

$$\mathrm{ROO^{\bullet} + AH \rightarrow ROOH + A^{\bullet}} \quad (1)$$

In the continued research for new improved antioxidants, nanomaterials represent one of the most promising frontiers. Some nanomaterials, such as melanin,[3] V_2O_5 nanowires[4] and cerium oxide[5] nanoparticles, show intrinsic redox activity that is often associated with radical trapping. Besides, redox inactive nanomaterials can be transformed into antioxidants by grafting low molecular weight antioxidants on them to obtain materials with improved characteristics. For instance, a covalent link between gallic acid (a food-grade antioxidant) and SiO_2 nanoparticles (SiO_2NPs) was proposed for reducing its leaching and volatility, and this material showed radical trapping activity toward the 1,1-diphenyl-2-picrylhydrazyl (DPPH•) radical.[6] Some of us recently demonstrated that carbon-coated cobalt nanomagnets decorated by α-tocopherol units are able to effectively counteract the autoxidation of organic substrates, and can be efficiently controlled by an external magnet.[7] Nanomaterials can also serve as carriers for controlled release of antioxidants. For instance, bio-degradable NPs have been used to improve the bioavailability of natural antioxidants such as epigallocatechin gallate, curcumin and quercetin.[8–10]

In this context, halloysite nanotubes (HNTs), a natural aluminosilicate clay, represent a versatile nanosized scaffold because chemicals can be loaded in the inner lumen, or grafted on both surfaces.[11–15]

[a] University of Palermo, Department STEBICEF, section Chemistry, Viale delle Scienze, Ed. 17, I-90128 Palermo, Italy. E-mail: serena.riela@unipa.it
[b] University of Bologna, Department of Chemistry "G. Ciamician", Via S. Giacomo 11, I-40126 Bologna, Italy. E-mail: riccardo.amorati@unibo.it
[c] University of Palermo, Department of Physic and Chemistry, Viale delle Scienze, Parco d'Orleans II, Ed. 17, 90128 Palermo, Italy

† Electronic supplementary information (ESI) available: FT-IR and TGA of novel materials, examples of UV traces for experiments with DPPH•, release profile of quercetin from HNT/Que, examples of numerical fittings of oxygen uptake kinetics. See DOI: 10.1039/c6tb00126b

HNTs are a biocompatible and low cost material, with a hollow tubular structure (*ca.* 1 μm in length and 80 nm in external diameter), consisting of siloxane groups on the outer surface and aluminol at the innermost surface. Therefore, the different inner and outer compositions of these materials allow exploiting different chemistry on either surface. External grafting has recently been tested by some of us in the case of curcumin, with the aim of obtaining controlled release,[14,16] while antioxidant loading on the inner lumen has previously been reported in the case of a diarylamine for rubber stabilization,[17] and in the case of natural phenolic antioxidants such as curcumin,[18] silibinin[19] and resveratrol,[20] to obtain controlled delivery systems.

Despite the large variety of currently known antioxidants,[2] several challenges still exist in specific applications such as in food technology,[21] pharmaceutical and cosmetics technology, or for biomedical applications, namely: (a) the potential toxicity of several antioxidants;[22] (b) antioxidant leaching or migration to unwanted compartments,[23] which is a major challenge in food preservation[24] and food packaging;[6] (c) their thermal stability[25] and sensitivity to atmospheric oxygen that causes limited performance or loss of performance with time;[26] (d) the browning of polyphenolic antioxidants,[27] which might occur either enzymatically or non-enzymatically.[28]

For such applications the advantage of HNT-based antioxidants over conventional systems is clear: (a) halloysite is a natural material with demonstrated low toxicity both *in vitro*[29] and *in vivo*[30] and could help reduce the toxicity of small molecule antioxidants, either carried or grafted, by decreasing their steady-state concentration in the system; (b) by carrying the antioxidants, halloysite would reduce their migration and leaching; additionally, antioxidants loaded in the inner cavity might be preserved from undesired reactions such as (c) degradation under ambient O_2, or (d) other unwanted reactions like polyphenol browning.

With the aim of further improving the usefulness and versatility of HNT-based antioxidants, we have devised the synthesis of novel HNT nanomaterials, in which different phenolic antioxidants are, for the first time, both loaded in the inner lumen and grafted on the outer surface. Indeed, the combining of different antioxidant functions on the same nanostructured material would sum up the advantages outlined in points (a)–(d) and offer distinctive additional advantages, *i.e.* (e) increase the load of antioxidants hence the duration of protection, and (f) exploit any synergism between different antioxidants.

Synergism among antioxidants is a well known behaviour for some small-molecule compounds,[31] which is usually aimed at in the design of antioxidant systems for specific applications.[32,33] Nonetheless this approach has never been rationally explored in nanoantioxidants.

Herein we report the synthesis and characterization of such a novel HNT-based antioxidant. Trolox, a mimic of α-tocopherol bearing a carboxylic group (see Scheme 1), was chosen as the surface exposed antioxidant because of its known high reactivity with radicals.[6] The natural polyphenol quercetin was instead loaded in the inner lumen, because of its renown importance as a radical trapping agent[34] and as a bioactive compound to counteract oxidative stress in many pathologies.[35] The synergism between the two functionalities and the performance of this novel material have been investigated using both the reaction with DPPH$^{\bullet}$ radicals (see Scheme 2) and inhibited autoxidation studies of two model organic substrates in solvents of different polarities.

Results and discussion

Synthesis of HNT–Trolox nanomaterials

HNT bearing Trolox units was prepared according to the synthetic route shown in Scheme 1. As previously reported, halloysite nanotubes were reacted with 3-azidopropyltrimethoxysilane in toluene at reflux, affording HNT–N_3, which represents a versatile starting point for subsequent functionalizations.[18] The reduction of HNT–N_3 with PPh_3 gave amino-functionalized HNT–NH_2[14] and after the work up, the NH_2 group loading, estimated by TGA, was *ca.* 1.5 ± 0.1 wt%.

The synthesis of HNT–Trolox was carried out by *N*,*N*′-dicyclohexylcarbodiimide-catalyzed condensation of Trolox to HNT–NH_2 by forming an amide bond that afforded a material with a loading of 8.8 ± 0.1 wt% with respect to HNT–NH_2. The new material was characterized by FT-IR spectroscopy, TGA and SEM measurements. The FT-IR spectra of HNT–Trolox, Trolox and pristine HNT are

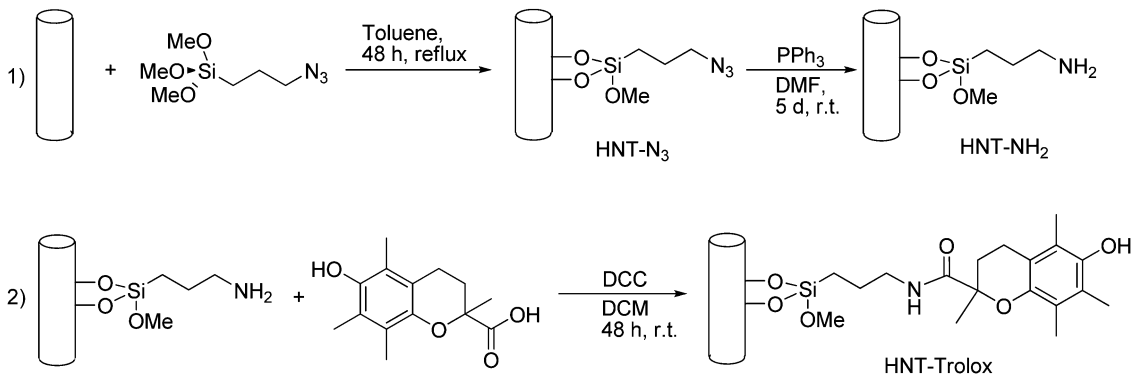

Scheme 1 Schematic representation of the synthesis of HNT–Trolox nanomaterials.

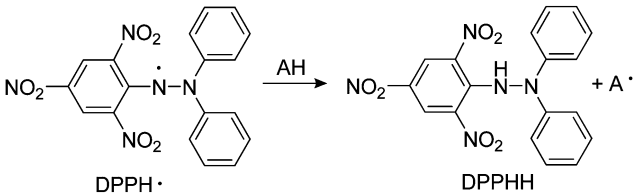

Scheme 2 Reaction of DPPH• with antioxidants.

illustrated in Fig. 1. The assignments for the bands of the pristine components can be done on the basis of literature data for HNT[13,36–38] and Trolox.[39] In particular, HNTs show two bands at 3622 and 3693 cm^{-1} corresponding to the O–H stretching of inner hydroxyl groups and outer surface hydroxyl groups, respectively.[36–38] Additionally a broad signal at 1640 cm^{-1} is attributed to the H–O–H bending of H-bonded water on the halloysite structure,[36] which corresponds to the broad O–H stretching signal at 3550 cm^{-1}. Apical Si–O and Si–O–Si stretching vibrations provided the bands at 1115 and 1031 cm^{-1}, respectively. The bands at 753 and 690 cm^{-1} derive from the perpendicular Si–O stretching vibration. The O–H deformation vibration of inner Al–O–H groups generates the band at 912 cm^{-1}. The FT-IR spectrum of Trolox shows an intense characteristic band at *ca.* 3550 cm^{-1} due to the O–H stretching of H-bond associated phenol, while the bands at 3015 and 2982 cm^{-1}, 2929 and 2837 cm^{-1} and 2962 cm^{-1} are related to unsaturated CH, saturated CH_2 and CH_3 moieties, respectively, of the Trolox molecule. A very broad signal at 3100 cm^{-1} that fuses with the C–H stretching region is due to the stretching of the H-bonded carboxylic O–H. In addition, the characteristic band at 1720 cm^{-1} is ascribed to the carboxylic C=O group. The hybrid material presents the characteristic bands of both HNT and Trolox with two main variations: the shift of the carbonyl group from 1720 cm^{-1} to 1630 cm^{-1} and the disappearance of the broad signal of the C(O)O–H stretching at 3100 cm^{-1}. These variations confirm the covalent grafting of Trolox to HNT–NH_2, and exclude the presence of adsorbed[40] Trolox on the surface or in the inner lumen of the nanotubes.[41]

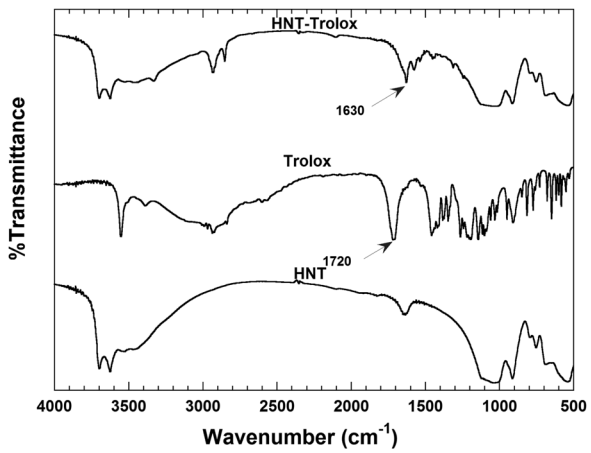

Fig. 1 FT-IR spectra of pristine HNT, Trolox and HNT–Trolox nanomaterials.

Thermogravimetric analyses (TGA) were performed on the pristine and on the hybrid nanomaterials (thermogravimetric and derivative thermogravimetric curves are provided in the ESI†). Trolox showed a two-step degradation process, with a fast followed by a slow degradation process. The hybrid nanomaterial had TGA profiles similar to HNT except for the thermal degradation of grafted Trolox. After the subtraction of the HNT signal HNT–Trolox presents a mass loss *vs.* temperature profile corresponding to that of pristine Trolox (Fig. 2). This finding confirms that Trolox is attached on the external surface as its thermal stability is not significantly altered upon combination with HNTs, similarly to previous observations in other surface-grafted clay materials.[42,43] From the mass change values it is possible to estimate the amount of Trolox grafted on the HNT surface as 10.3 ± 0.1 wt%. In addition to TGA analysis, to estimate the amounts of Trolox, we performed fluorescence spectroscopy experiments in methanol. The HNT–Trolox hybrid showed a characteristic fluorescence spectrum for Trolox[44] (see spectra in ESI†) and a quantitative analysis allowed calculation of a loading of 10.4 wt%, which is in straightforward agreement with the TGA data.

The dimension of HNT–Trolox was assessed by dynamic light scattering (DLS) studies. The results, reported in Fig. 3, show that the HNT–Trolox particles in MeCN are distributed between two populations: the first with a hydrodynamic diameter approximately around 340 nm, quite similar to the pristine HNTs, the second around a value of 1100 nm. The latter population is reasonably constituted by clusters of 3–4 HNT–Trolox units, due to hydrophobic attractions between the Trolox molecules that are covalently linked on the surface of the HNT. It is worth noting that the two populations are very well separated.

The surface morphology of HNT–Trolox was imaged by SEM. It clearly appears that the tubular shape of the halloysite is

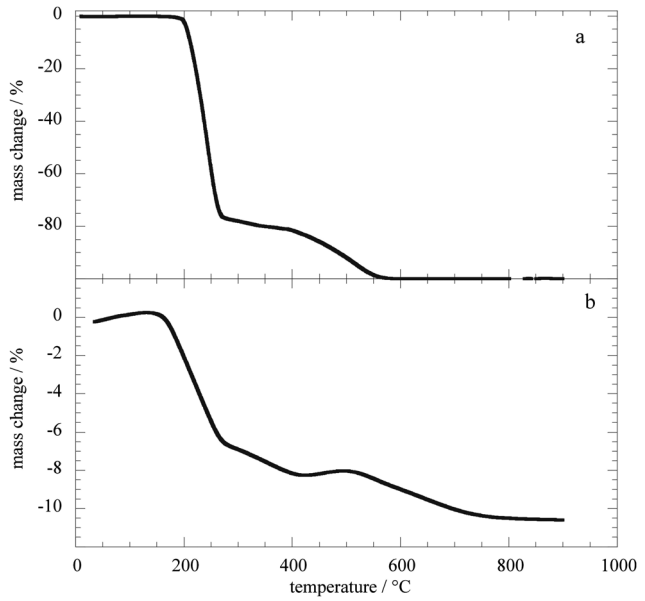

Fig. 2 Thermogravimetric curves of Trolox (a) and HNT–Trolox after HNT signal subtraction (b).

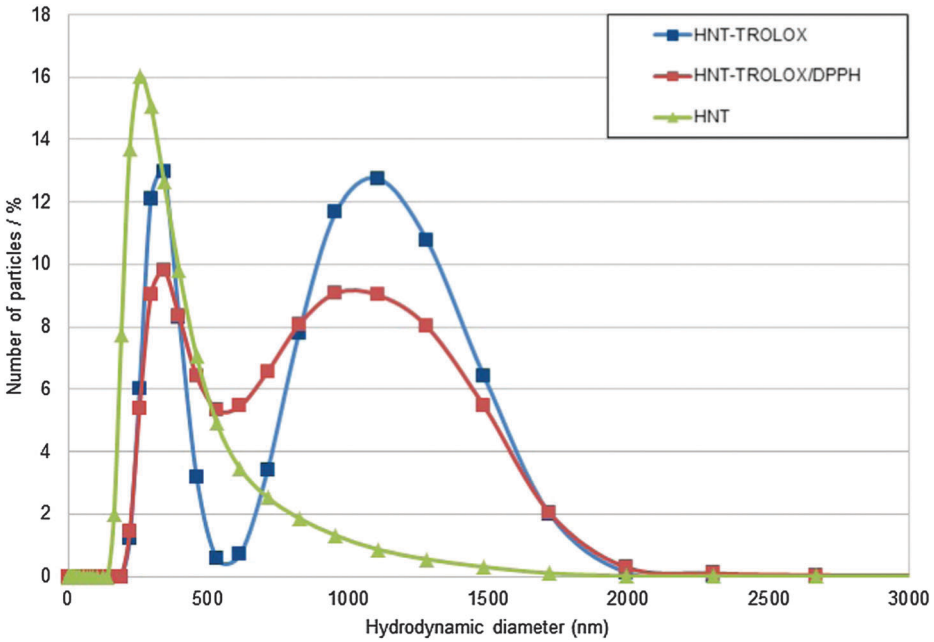

Fig. 3 Hydrodynamic diameter distribution by DLS measurements in MeCN for pristine HNT, HNT–Trolox and HNT–Trolox treated with DPPH• (HNT–Trolox/DPPH).

maintained after Trolox grafting (Fig. 4). Furthermore the images show that HNT–Trolox has a rather compact structure where nanotubes seem to be glued together as a result of interactions established by the organic structures grafted on the external surface.

Loading of quercetin into HNT–Trolox nanotubes

With the aim of combining two or more antioxidant molecules with synergistic effects, we loaded the HNT–Trolox nanomaterial with quercetin (HNT–Trolox/Que), a polyphenolic compound that can interact with HNT lumen.[19]

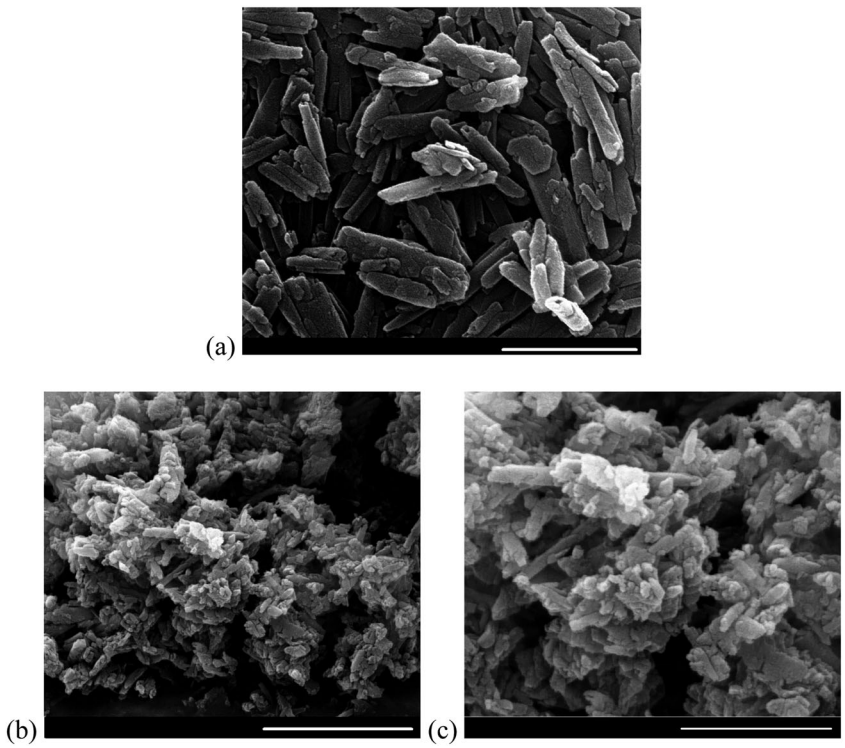

Fig. 4 SEM images of pristine HNT (a) and of HNT–Trolox (b and c) showing the nanotubular structure ((c) enlargement of the central part of (b)), scale bars: (a) 1 μm (b) 2 μm; (c) 1 μm.

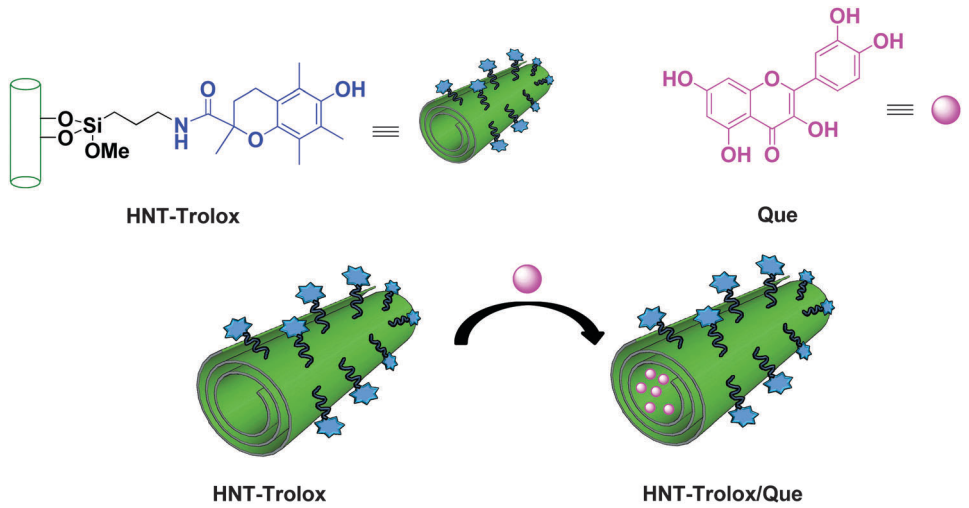

Fig. 5 Schematic representation of quercetin loading into HNT–Trolox.

Loading quercetin into HNT–Trolox was carried out by vacuum cycling of a HNT–Trolox suspension in a quercetin solution (Fig. 5). This cycle was repeated several times in order to obtain the highest loading efficiency. After loading, the HNT–Trolox/Que complex was washed with water in order to remove free quercetin. Quercetin loaded HNT without Trolox, HNT/Que, was similarly prepared as a reference material. The loading efficiencies of HNT/Que and HNT–Trolox/Que were estimated spectrophotometrically after extraction with methanol. The amount of Que loaded in the HNT lumen, expressed as the percent amount of drug in the final composite, was *ca.* 2 wt%.

The composite solid HNT–Trolox/Que was characterized by TGA. The thermoanalytical curves clearly show the successful loading of the molecule (see ESI† for full details). Given that quercetin degraded with a null residual at 900 °C, we calculated that the hybrid HNT–Trolox is able to incorporate 2.2 ± 0.1 wt% of quercetin by mass loss difference, in agreement with the UV-vis results. It should be noted that the quercetin loading amount was unchanged for pristine HNTs. It is interesting to note that quercetin was thermally stabilized by loading into either HNTs or HNT–Trolox, as its thermal degradation curve was shifted toward higher temperature as compared to the native nanomaterial (Fig. 6).

This indicates that in the composite material quercetin is effectively loaded into the lumen. Thermal stabilization of quercetin also highlights the advantage of its loading into HNTs, particularly for applications in which heating might be involved, *e.g.* during industrial processing.

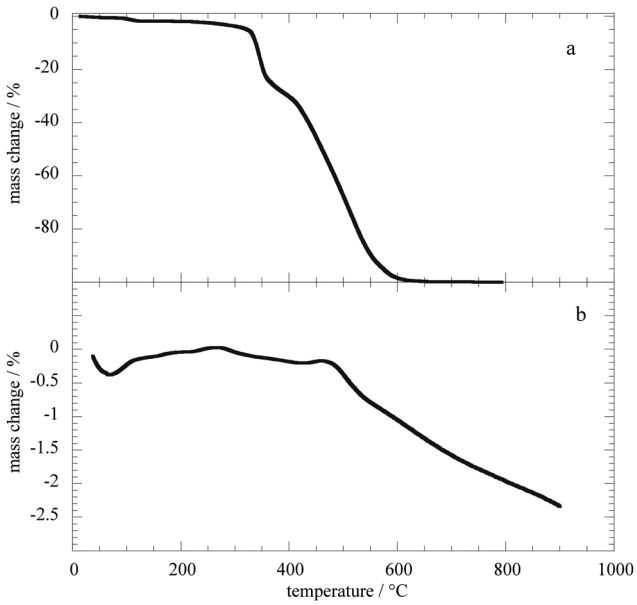

Fig. 6 Thermogravimetric curves for quercetin (a) and nanotubes loaded with quercetin after subtraction of nanotube signals (b).

Antioxidant activity

Antioxidant activity of HNT–Trolox, HNT/Que and HNT–Trolox/Que was evaluated in comparison with native Trolox and quercetin, by measuring the rate constant (k_{inh}) for the reaction with peroxyl radicals (ROO$^\bullet$), which are responsible for the propagation step of peroxidation processes in most natural and man-made materials.[1] The values of k_{inh} (eqn (6), where AH is the antioxidant) were determined by studying the inhibition of the thermally initiated autoxidation of either cumene or styrene (RH), chosen as reference oxidizable substrates (eqn (2)–(7)), under controlled conditions, using chlorobenzene or acetonitrile as solvents, which were used to simulate the apolar or mildly polar environments that can be found in the interior of biological membranes or in easily-oxidizable lipid-rich foods.[45]

$$\text{Initiator} \xrightarrow{R_i} \text{R}^\bullet \quad (2)$$

$$\text{R}^\bullet + \text{O}_2 \rightarrow \text{ROO}^\bullet \quad (3)$$

$$\text{ROO}^\bullet + \text{RH} \xrightarrow{k_p} \text{R}^\bullet + \text{ROOH} \quad (4)$$

$$2\text{ROO}^\bullet \xrightarrow{2k_t} \text{non radical products} \quad (5)$$

$$ROO^{\bullet} + AH \xrightarrow{k_{inh}} ROOH + A^{\bullet} \quad (6)$$

$$A^{\bullet} + ROO^{\bullet} \rightarrow \text{non radical products} \quad (7)$$

The reactions were performed at 303 K using azobisisobutyronitrile (AIBN) as an initiator, and were followed by monitoring the oxygen consumption in an oxygen-uptake apparatus based on a differential pressure transducer. In the presence of antioxidants, the oxidation of the substrate and oxygen consumption are much slower than in their absence, and a clear inhibition period is observed. The rate constant for the reaction with ROO$^{\bullet}$ radicals could be obtained from the rate of O_2 consumption during the inhibited period from the known chain-propagation and chain-termination rate constants, k_p and $2k_t$ respectively, for the autoxidation of styrene or cumene, as detailed in the experimental section. Styrene oxidizes quickly, similarly to the natural lipid methyl linoleate, and it is best suited to measure k_{inh} values in the range 10^5–10^7 M^{-1} s^{-1}. Cumene oxidizes slowly and can be used to measure the k_{inh} values in the range 10^3–10^5 M^{-1} s^{-1}.[46] The number of radicals trapped by each antioxidant molecule (n) was obtained from the length of the inhibition period, by comparison with the reference antioxidant 2,2,5,7,8-pentamethyl-6-chromanol (PMHC), a model for the physiological antioxidant α-tocopherol, for which n = 2.[45] In the case of HNT–Trolox and HNT/Que, the molar concentration of antioxidants (Trolox and quercetin, respectively) could be obtained from the amount (w/v) of nanomaterial in the sample and loading determined by TGA.

To get a deeper insight into the radical trapping by novel hybrid materials, we studied also the reaction with the stable coloured 1,1-diphenyl-2-picrylhydrazyl (DPPH$^{\bullet}$) radical, as the purple free radical is transformed by reductants to the yellow hydrazine DPPHH through a formal hydrogen atom transfer reaction (see Scheme 2).[34,47,48] After mixing an excess of DPPH$^{\bullet}$ with the investigated compounds in MeCN, the absorbance of DPPH$^{\bullet}$ at 517 nm decreased, while the addition of pristine HNTs did not modify the absorption spectrum (see ESI†). The number of DPPH$^{\bullet}$ radicals quenched by each molecule of antioxidant, free or linked to HNT, was measured from absorbance readings after 20 h of reaction, to ensure that the kinetics of release of the antioxidant from the nanoclay is not the limiting factor.

Trolox and quercetin

First, the antioxidant activities of Trolox and quercetin alone were analyzed to check the behaviour in the absence of HNTs. In Fig. 7A, it is evident that both Trolox and quercetin are effective inhibitors of the autoxidation of styrene in the apolar solvent PhCl, with k_{inh} values of 9.8×10^5 and 1.0×10^6 M^{-1} s^{-1}, and stoichiometric coefficients of 1.8 and 1.9, respectively, in good agreement with previous results.[46]

Parallel experiments performed by using cumene as an oxidizable substrate are summarized in Fig. 7B. As expected, Trolox and quercetin completely inhibited the autoxidation of cumene (traces a and b), but in the case of quercetin the stoichiometric coefficient was much larger than that recorded in the autoxidation of styrene, which is about 4. This result is consistent with the capability of quercetin to efficiently trap two ROO$^{\bullet}$ radicals by the catechol B ring, and two other radicals, more slowly, by the resorcinol A ring, as depicted in Scheme 3. The k_{inh} value relative to the second process could be distinguished in cumene as 5.2×10^4 M^{-1} s^{-1} (see Table 1).

Upon changing the solvent from PhCl to MeCN, k_{inh} values decrease (see Table 1), due to the formation of H-bonds between the MeCN and the reactive OH groups.[46] Comparison between traces b and c in Fig. 7B shows that in MeCN the inhibiting effect of quercetin is smaller than in PhCl, and only the trapping of the first two ROO$^{\bullet}$ radicals is visible.

Results obtained with the DPPH$^{\bullet}$ radical confirmed the stoichiometric coefficients found in the autoxidation experiments. As shown in Table 2, the stoichiometry of DPPH$^{\bullet}$ radical trapping by Trolox in acetonitrile was 2, and that of quercetin was about 4.

HNT–Trolox nanotubes

Any of the novel HNT-based antioxidants showed good protection of styrene and cumene autoxidation, as reported in Fig. 8. While pristine HNTs had no effect on autoxidation (see traces (a)), HNT–Trolox showed a strong inhibition corresponding to k_{inh} of 1.1×10^6 M^{-1} s^{-1} in PhCl and 9×10^4 M^{-1} s^{-1} in MeCN. These two values are very similar to those displayed by Trolox itself and indicate that the grafting on the HNT surface does not significantly modify the reactivity of the phenolic OH with

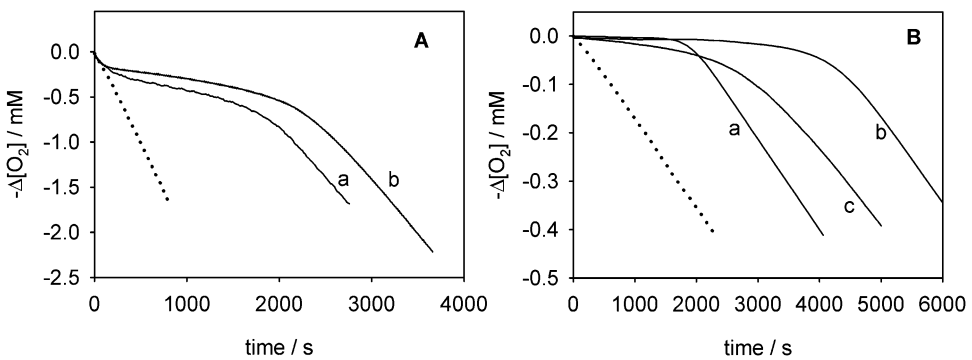

Fig. 7 Inhibition of the autoxidation of styrene (A) or of cumene (B) in chlorobenzene by either Trolox (a) or quercetin (b), both 2.5 μM. Trace (c) is the inhibition given by 2.5 μM quercetin in acetonitrile. Dotted lines show the autoxidation course without antioxidants.

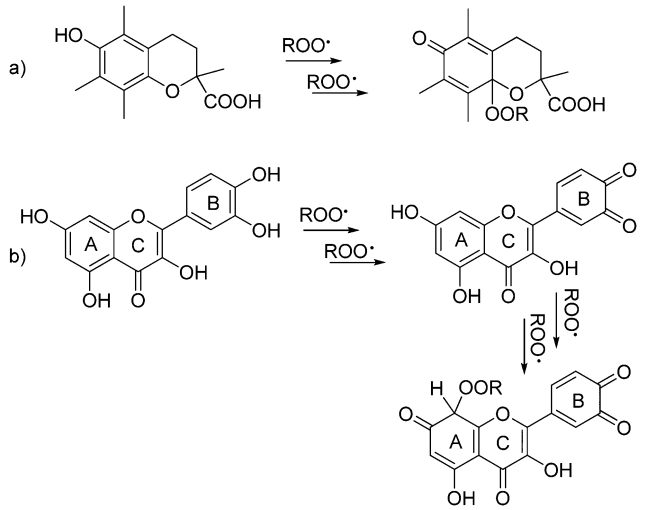

Scheme 3 Stoichiometry of radical trapping by Trolox (a) and quercetin (b).

ROO• radicals. On the other hand, the stoichiometry of radical trapping of HNT–Trolox, calculated on the basis of the amount of Trolox units loaded on HNTs, was approximately half of that recorded for Trolox alone (see Table 1).

Also, DPPH• experiments confirmed that the stoichiometry of HNT–Trolox is roughly half than that of Trolox (see Table 2), thus suggesting that this behaviour does not depend on the radical employed. Similar reductions of the stoichiometry after grafting an antioxidant on a nanoparticle was previously evidenced in the case of gallic acid linked to silica NPs[6] and Trolox linked to cobalt NPs.[7] As previously suggested by Deligiannakis *et al.*, this effect is reasonably due to the preference of bound antioxidants for self-decay than for trapping a second radical.[6] The self-decay of phenoxyl radicals was also reported to occur between antioxidant units belonging to different nanoparticles, leading to agglomeration and to an increased hydrodynamic radius after the reaction with free radicals.[6] We tested this effect by performing a DLS experiment on a sample of HNT–Trolox after its reaction with excess of DPPH•. The result, reported in Fig. 3, shows that the peaks at 340 and 1100 nm of HNT–Trolox are less separated, because of the formation of some aggregates with an intermediate size.

Table 2 Number n of moles of DPPH• reduced per mole of antioxidant (free or linked), in acetonitrile at 298 K (mean ± SD, N = 3)

Antioxidant	n
Trolox	2.0 ± 0.2
Quercetin	4.0 ± 0.2
HNT–Trolox	1.3 ± 0.2
HNT/Que	3.8 ± 0.2
HNT–Trolox/Que[a]	Expected: 1.8 Found: 2.8 ± 0.2

[a] Molar ratio trolox/quercetin = 0.79/0.21.

It can therefore be concluded that the reaction with DPPH• induces a slight aggregation of HNT–Trolox, reasonably due to the cross-linking of the Trolox units.

HNT/Que nanotubes

In the case of HNT/Que, the apparent antioxidant activity obtained from the slopes of the oxygen uptake plots was rather low (k_{inh} of 1.7×10^4 M^{-1} s^{-1} in PhCl and 2.9×10^3 M^{-1} s^{-1} in MeCN), as compared to that of quercetin itself, both in PhCl and in MeCN (Fig. 8 traces (b) and Table 1). We explain this result on the basis of the low solubility and consequently the slow release of quercetin from the inner lumen of HNTs, so that only a small fraction of it is available for the reaction with ROO• radicals at any given time during the course of autoxidation. To test this hypothesis, we performed autoxidation studies inhibited by "free" quercetin in the presence of pristine HNTs, and we found that in PhCl the nanoclay actively removes the antioxidant from the solution, reducing its apparent k_{inh} and n values (see Table 1). On the other hand, experiments with DPPH• showed that the stoichiometry of radical trapping of HNT/Que was very similar to that of quercetin alone in acetonitrile, reasonably because the long reaction time used in these experiments (20 h) and the excess of radical used, allowed quercetin to be almost completely released from HNTs (*vide infra*).

In order to deconvolute the kinetics of release of quercetin from the kinetics of peroxyl radical trapping during inhibited autoxidation, the oxygen uptake plots were analysed by numerical fitting[49] using kinetic simulation software.[50] This analysis identified three sites for quercetin binding to HNT, L_1, L_2 and L_3,

Table 1 Antioxidant activity (rate constant for the reaction with ROO• radicals, k_{inh}) and the number of radicals trapped by each antioxidant molecule (n) measured in inhibited autoxidation experiments at 303 K (mean ± SD, N = 3)

	PhCl		MeCN	
Antioxidant	k_{inh}/M^{-1} s^{-1}	n	k_{inh}/M^{-1} s^{-1}	n
Trolox	$(9.8 \pm 0.5) \times 10^5$	1.8 ± 0.1	$(1.6 \pm 0.2) \times 10^5$	1.6 ± 0.2
Quercetin	$(1.0 \pm 0.1) \times 10^6$ [a]	1.9 ± 0.1	$(1.5 \pm 0.2) \times 10^4$ [a]	1.9 ± 0.1
HNT	No inhib.	0	No inhib.	0
Quercetin + HNT[b]	$(6.5 \pm 0.2) \times 10^5$	1.3 ± 0.2	—	—
HNT–Trolox	$(1.1 \pm 0.1) \times 10^6$	0.8 ± 0.1	$(9 \pm 2) \times 10^4$	1.2 ± 0.1
HNT/Que	$(1.7 \pm 0.1) \times 10^4$ [c]	1.3 ± 0.1	$(2.9 \pm 0.3) \times 10^3$ [c]	1.4 ± 0.1
HNT–Trolox/Que	$(1.1 \pm 0.1) \times 10^6$	1.5 ± 0.2	$(8 \pm 2) \times 10^4$	1.9 ± 0.2

[a] Measured for the 1st reactive –OH; the value determined for the 2nd reactive –OH is k_{inh} $(5.2 \pm 0.1) \times 10^4$ M^{-1} s^{-1} (n = 1.6 ± 0.1) and k_{inh} = $(4.8 \pm 0.4) \times 10^3$ M^{-1} s^{-1} (n = 1.9 ± 0.1) in PhCl and MeCN respectively. [b] The reaction mixture contained pristine HNT (0.1 mg mL^{-1}) and variable amount of free quercetin. [c] Apparent inhibition constant; actual k_{inh} values from numerical fittings were 1.0×10^6 and 1.5×10^4 M^{-1} s^{-1} M^{-1} s^{-1} in PhCl and MeCN, respectively.

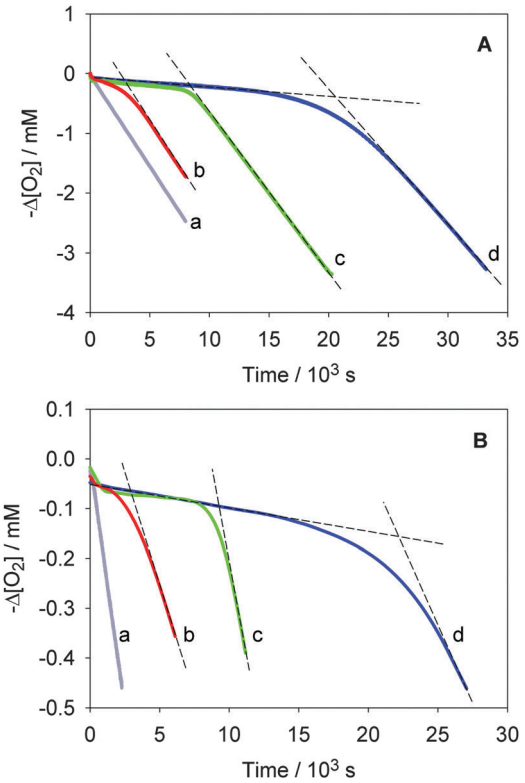

Fig. 8 Inhibition of the autoxidation of cumene in acetonitrile (A) or chlorobenzene (B) by 0.1 mg mL^{-1} of: pristine HNT (a), HNT/Que (b), HNT–Trolox (c) and HNT–Trolox/Que (d).

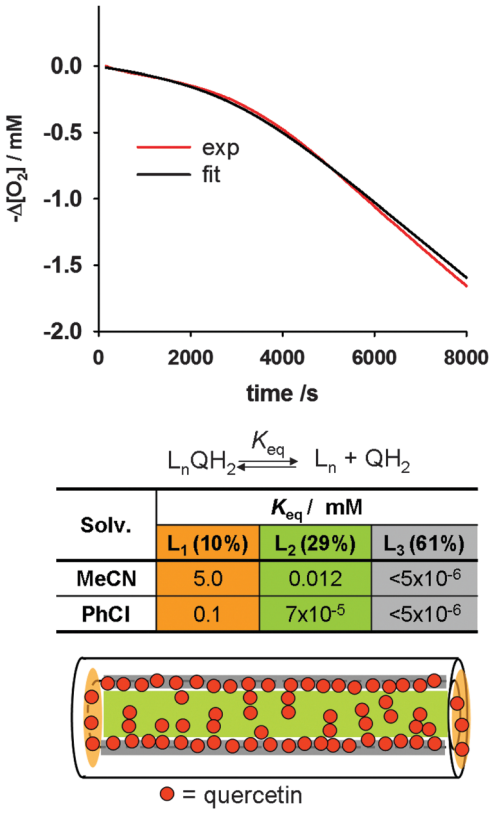

Solv.	K_{eq} / mM		
	L_1 (10%)	L_2 (29%)	L_3 (61%)
MeCN	5.0	0.012	<5x10^{-6}
PhCl	0.1	7x10^{-5}	<5x10^{-6}

Fig. 9 Example of the numerical analysis of O_2 consumption traces. The release of quercetin (QH_2) was simulated by assuming that it is bound to three sites, with low (L_1), medium (L_2) and high (L_3) affinity.

with decreasing ease of desorption by the solvent, accounting for 10%, 29% and 61%, of the loaded quercetin. In the experiments in chlorobenzene, quercetin bound to L_1 (see Fig. 9) is rapidly released during the time-course of autoxidation, whereas the quercetin bound to L_2 is only partially released. In acetonitrile, quercetin bound to sites L_1 and L_2 is rapidly and almost completely released, while that bound to the high affinity site L_3 is negligibly released. Halloysite has specific surface area of 65 m^2 g^{-1};[11] taking the average length of 770 nm and an external diameter of 73 nm,[51] considering that its cavity accounts for about 10% its volume[51] and quercetin has a molecular surface of about 70 Å^2, it can be calculated that a monolayer of quercetin adsorbed in the inner lumen would account for about 1.5 wt%, in line with previous calculations for the load of monolayer surfactants.[51,52] This calculated value, which would correspond to 63% of the quercetin loading into HNTs, is equivalent to the value of 61% obtained form our fittings for the binding site L_3. We suggest that the high affinity site corresponds to the surface of the inner lumen, which is expected to bind the mildly acidic quercetin through strong H-bonding and Coulombic interactions, from which it is slowly released following solid–liquid reversible adsorption–desorption kinetics.[53] The intermediate affinity L_2 site corresponds to the solid drug accumulated in the hollow space inside HNTs, which is not easily reached by solvents, whereas the fast release site L_1 corresponds to the quercetin absorbed at the ends of HNTs, as depicted in Fig. 9.

The equilibrium constants for the release of quercetin from the three binding sites are summarized in Fig. 9 (see ESI† for full details). HNTs serve as controlled release systems for loaded quercetin, which displays the typical reactivity with peroxyl radicals after release in solution: k_{inh} of 1.0 × 10^6 M^{-1} s^{-1} in PhCl and 1.5 × 10^4 M^{-1} s^{-1} in MeCN.

This explanation was supported by UV-vis spectroscopy measurements in MeCN (see ESI†), which showed a fast release of 35% quercetin in about 2 h, followed by a much slower release which accounted for only an additional 2% of quercetin released after 20 h.

Under these conditions, experimental data points can be analyzed using the following equation:

$$\mathrm{Abs}(t) = A_1[1 - e^{(-k_1 t)}] + k_0 t \quad (8)$$

comprising the sum of an exponential and a linear term. This indicates the superimposition of two distinct processes, namely a relatively faster first-order (k_1 = 0.077 ± 0.007 min^{-1}) and a much slower zero-order release (k_0 = 0.0022 ± 0.0009 min^{-1}).

These results suggest that HNT/Que acts as a dynamic reservoir of quercetin, whose release in solution is regulated by its consumption by oxidizing radicals. This also explains the higher apparent stoichiometric factor recorded for reaction with the persistent DPPH• radical (see Table 2), which "waits" in solution until all quercetin has been released, by shifting its equilibrium of binding with the nanotube.

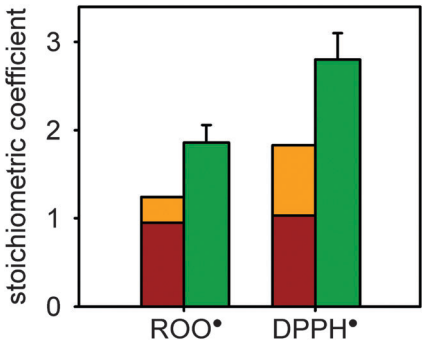

Fig. 10 Synergic effect in HNT–Trolox/Que: experimental stoichiometric coefficient in MeCN (green bars, ± SD, N = 3) compared to theoretic one, as calculated from the sum of contributions of HNT–Trolox (red bars) and HNT/Que (orange bars) alone.

HNT–Trolox/Que hybrid nanotubes

HNT–Trolox/Que showed a very strong antioxidant activity both in PhCl and in MeCN, as can be inferred from traces (d) in Fig. 8. Interestingly, both the inhibition length and the efficacy were higher than the sum of effects observed for HNT–Trolox and HNT/Que, indicating the occurrence of synergy between the two antioxidant functions in HNT–Trolox/Que. In fact, the number of theoretical radicals trapped by a solution of HNT–Trolox/Que (with a molar ratio 0.79/0.21 for Trolox/Quercetin) without synergic effect would be n_{Theor} = 1.24 in MeCN, using n = 1.2 for HNT–Trolox and n = 1.4 for HNT/Que; instead the radicals trapped by our new three-component system are n_{Exp} = 1.9 in MeCN, which is greater than n_{Theor}, as shown in Fig. 10. Similarly, in PhCl n_{Exp} = 1.5 is higher than the theoretical value n_{Theor} = 0.91.

The synergic effect is also observed in DPPH• experiments: radicals trapped by HNT–Trolox/Que are n_{Exp} = 2.8 in MeCN, a value much greater than n_{Theor} = 1.9 (see Fig. 10), which can be calculated using n = 1.3 for HNT–Trolox and n = 3.8 for HNT/Que. Interestingly, the length of the antioxidant activity of mixtures of Trolox and quercetin without HNT was the sum of the contributions of the single components (see ESI†). Synergic antioxidant effect has previously been observed for antioxidant mixtures in solution and is typical of a main (*i.e.* more active) antioxidant AH being regenerated from its oxidation products by a co-antioxidant Co-AH acting as a sacrificial reducing agent[33,54] as simplified in eqn (9) and (10).

$$\mathrm{AH} + \mathrm{ROO}^{\bullet} \rightarrow \mathrm{A}^{\bullet} + \mathrm{ROOH} \quad (9)$$

$$\mathrm{Co{-}AH} + \mathrm{A}^{\bullet} \rightarrow \mathrm{Co{-}A}^{\bullet} + \mathrm{AH} \quad (10)$$

In the case of the HNT–Trolox/Que antioxidant system, kinetic analysis indicates that Trolox grafted on the HNT surface acts as the main antioxidant (AH), which is immediately available for fast reaction with peroxyl radicals, then it is regenerated by quercetin, the co-antioxidant, which is slowly released from the nanotube cavity. However, as the grafting of Trolox on HNTs reduces its stoichiometric coefficient, similarly to all known examples of surface-bound antioxidants, the effect of loaded quercetin appears that of restoring the pristine radical trapping ability of Trolox. Therefore, the synergic interplay between the two antioxidant functions is a distinctive advantage of this novel nano-antioxidant since it is able to afford rapid protection from oxidation using externally exposed Trolox, combined with prolonged undiminished efficacy due to the slow release of loaded quercetin, which is mainly regulated by its rate of consumption to regenerate the main antioxidant. An account of the different radical reactions involved in the antioxidant activity of HNT–Trolox/Que is reported in Scheme 4.

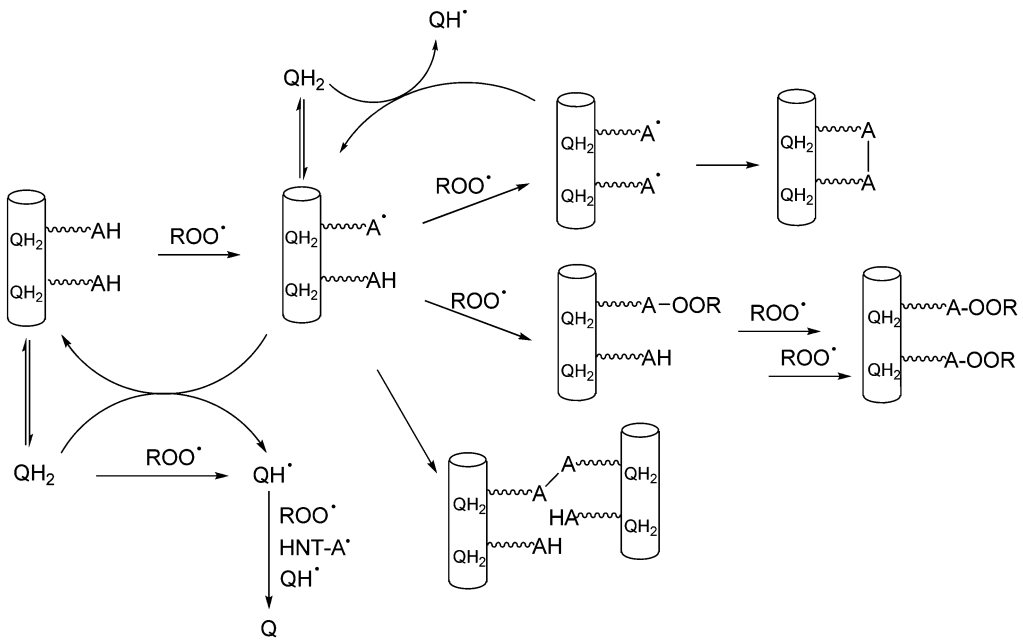

Scheme 4 Mechanism explaining the antioxidant behaviour of HNT–Trolox/Que, where Trolox is identified as AH and quercetin as QH_2.

Conclusions

HNT–Trolox/Que is a very effective antioxidant nanomaterial, endowed with complementary antioxidant functionalities displaying synergistic effects. To the best of our knowledge, this is the first example of a synergic nanoantioxidant. It also represents the prototype for a general design strategy expected to afford improved antioxidant halloysite nanotubes, in which one main phenolic antioxidant function (like Trolox) is exposed on the outer surface and is readily available to trap free radicals, whereas a second co-antioxidant (like quercetin) is loaded in the inner lumen and is slowly released to regenerate the main antioxidant and afford a prolonged synergistic protection. We have shown that both HNT–Trolox and HNT/Que are interesting and effective antioxidant materials, able to quench both DPPH$^{\bullet}$ and peroxyl radicals, protecting organic materials from autoxidation. However, their stoichiometry of radical trapping is less favourable than results obtained with the corresponding molecular antioxidants (*i.e.* ''free'' Trolox or quercetin); a similar unfavourable feature has previously been reported for nano-antioxidants built by functionalization of a nanosized scaffold with a phenolic compound.[6,7] In this respect we showed that HNT–Trolox/Que offers a distinctive advantage in that, due to the synergistic interplay among antioxidant functions, it offers extended protection with respect of materials endowed with a single antioxidant function.

Experimental section

Materials

Trolox ((±)-6-Hydroxy-2,5,7,8-tetramethylchromane-2-carboxylic acid), quercetin, styrene, cumene, AIBN were commercially available (Sigma Aldrich). Solvents were of the highest grade commercially available and were used as received. Styrene and cumene were percolated twice on an alumina column before use. AIBN was recrystallized from methanol and stored at −18 °C. All reagents needed for the functionalization (Sigma) were used without further purification.

Halloysite was purchased from Sigma-Aldrich. This material has an average tube diameter of 50 nm and an inner lumen diameter of 15 nm. A typical specific surface area of this halloysite is 65 $m^2\ g^{-1}$, a pore volume of ∼1.25 $cm^3\ g^{-1}$, a refractive index 1.54 and a specific gravity 2.53 g cm^{-3}.

Synthesis of HNT–Trolox

HNT–N_3 and HNT–NH_2 were prepared as previously reported.[14,18] (±)-6-hydroxy-2,5,7,8-tetramethylchromane-2-carboxylic acid (55 mg, 10 eq.) was suspended in CH_2Cl_2 (7.5 mL) and *N*,*N* dicyclohexylcarbodiimide (88 mg, 10 eq.) was added. The suspension was stirred under an argon atmosphere, at room temperature for 10 min. Afterwards HNT–NH_2 (250 mg) was quickly added. The mixture was left under stirring for 48 h. Then, the solvent was filtered off, the powder was rinsed with H_2O and, successively, with CH_2Cl_2 and finally dried at 80 °C under vacuum.

Loading of quercetin

To a dispersion of HNTs or HNT–Trolox in deionized water (5 mL), 1 mL of quercetin solution 10^{-2} M in ethanol was added. The suspension was sonicated for 5 min, at an ultrasound power of 200 W and at 25 °C and then was evacuated for 3 cycles. The suspension was left under stirring for 24 h at room temperature. After this time the powder was washed with water and then dried at 70 °C under vacuum. Loading was determined as follows: *ca.* 5 mg of HNTs or HNT–Trolox were carefully weighed and washed with methanol (25 mL). The quercetin concentration in solution was determined by UV-vis spectrometry using the Lambert–Beer law.

General procedures

Dynamic light scattering (DLS) measurements were carried out by means of a Zetasizer NANO-ZS (Malvern Instruments). The field-time autocorrelation functions were analyzed by the Inverse Laplace Transform (ILT), which provides the decay rates (Γ) of the diffusive modes. For the translational motion, the collective diffusion coefficient at a given concentration is $D_t = \Gamma/q^2$ where q is the scattering vector given by $4\pi n\lambda^{-1}\sin(\theta/2)$ with n being the acetonitrile refractive index, λ the wavelength (632.8 nm) and θ the scattering angle (173°). The hydrodynamic diameter (D_h) was calculated by means of the Stokes–Einstein relation. The thermogravimetric analyses were done by using a Q5000 IR apparatus (TA Instruments) under nitrogen flow of 25 $cm^3\ min^{-1}$ for the sample and 10 $cm^3\ min^{-1}$ for the balance at the heating rate of 10 °C min^{-1}. Temperature spanned from ambient to 900 °C.

FT-IR spectra in KBr were determined at room temperature in the spectral region 400–4000 cm^{-1} by means of an FT-IR spectrophotometer (Agilent Technologies Cary 630). An average of 30 scans per sample using a nominal resolution of 4 cm^{-1} was registered. An AESEM FEI QUANTA 200F microscope apparatus was used to study the morphology of the functionalized HNTs. Before each experiment, the sample was coated with gold under argon by means of an Edwards Sputter Coater S150A, in order to avoid charging under electron beam. Fluorescence experiments were carried out in a Fluoromax 4 (Jobin-Yvon) spectrofluorometer (right angle geometry, 1 cm × 1 cm quartz cell) at 25.0 (0.1 °C). The excitation wavelength was of 290 nm and the emission spectra were recorded from 300 to 500 nm. The widths of slits were set at 2 and 2 nm for excitation and emission, respectively. A long pass filter was used to suppress HNT scattered radiation. UV-vis spectra were performed using a Beckmann DU 650 spectrometer.

Antioxidant activity

The chain-breaking antioxidant activity of the title compounds was evaluated by studying the inhibition of the thermally initiated autoxidation of styrene (4.3 M) or cumene (3.5 M) in chlorobenzene or acetonitrile. Autoxidation experiments were performed by measuring the O_2 consumption using a gas-uptake recording apparatus built in our laboratory based on a Validyne DP15 differential pressure transducer.[55] In a typical

experiment, an air-saturated mixture of the oxidizable substrate and the solvent containing AIBN (0.025 M) was equilibrated with the reference solution containing also excess of 2,2,5,7,8-pentamethyl-6-chromanol in the same solvent at 30 °C. After equilibration, 50–150 μL of a concentrated solution of the antioxidant was injected into the sample flask, and oxygen consumption in the sample was measured. From the slope of oxygen consumption during the inhibited period (see Fig. 7 and 8), k_{inh} values were obtained by using eqn (11) while the n coefficients were determined from the length of the inhibited period (τ) by using eqn (12), from the known rate of radical production by AIBN (initiation rate, R_i).

$$\Delta[O_2]t = -\frac{k_p}{k_{inh}} \cdot [\text{cumene}] \cdot \ln\left(\frac{1-t}{\tau}\right) \quad (11)$$

$$n = \frac{R_i \cdot \tau}{[\text{antioxidant}]} \quad (12)$$

The k_p values of styrene and cumene at 303 K are 41 and 0.32 M^{-1} s^{-1}, respectively. The value of R_i was determined under each experimental condition by using 2,2,5,7,8-pentamethyl-6-chromanol (n = 2) as a reference.[45,46]

Determination of DPPH• scavenging

The reaction mixtures were prepared by adding to the DPPH• radical in acetonitrile (1.0×10^{-4} and 5.0×10^{-5} M) different concentrations of the investigated radical. The total volume of the reaction mixture was 2 mL. The absorption of DPPH• was determined by recording spectra in sequence until the absorbance was unchanged (20 h) and against a blank solution that contained only acetonitrile (λ_{max} = 517 nm, ε = 11 000 ± 50 M^{-1} cm^{-1}).[34] UV-vis spectra were recorded using a Jasco V-550 spectrophotometer.

Abbreviations

HNT	Halloysite nanotubes
ROO•	Alkylperoxyl radical
DPPH•	Diphenylpicrylhydrazyl radical
DLS	Dynamic light scattering
TGA	Thermo-gravimetric analysis
AIBN	2,2′-Azobis(isobutyronitrile)
NP	Nanoparticle

Acknowledgements

This work was supported by a grant to L. V., A. B., and R. A. from the Italian MIUR (PRIN 2010-2011 2010PFLRJR, PROxi project). L. V. and R. A. acknowledge funding from the University of Bologna (FARB project FFBO123154) and support from COST action CM1201. We also acknowledge support from the University of Palermo, PRIN 2010-2011 (prot. 2010329WPF), FIRB 2012 (prot. RBFR12ETL5), PON-TECLA (PON03PE_00214_1).

References

1 R. Amorati and L. Valgimigli, Advantages and limitations of common testing methods for antioxidants, *Free Radical Res.*, 2015, **49**, 633–649.
2 K. U. Ingold and D. A. Pratt, Advances in radical-trapping antioxidant chemistry in the 21st century: a kinetics and mechanisms perspective, *Chem. Rev.*, 2014, **114**, 9022–9046.
3 E. Kim, Y. Liu, W. T. Leverage, J.-J. Yin, I. M. White, W. E. Bentley and G. F. Payne, Context-dependent redox properties of natural phenolic materials, *Biomacromolecules*, 2014, **15**, 1653–1662.
4 A. A. Vernekar, D. Sinha, S. Srivastava, P. U. Paramasivam, P. D'Silva and G. Mugesh, An antioxidant nanozyme that uncovers the cytoprotective potential of vanadia nanowires, *Nat. Commun.*, 2014, **5**, 5301.
5 S. S. Lee, W. Song, M. Cho, H. L. Puppala, P. Nguyen, H. Zhu, L. Segatori and V. L. Colvin, Antioxidant properties of cerium oxide nanocrystals as a function of nanocrystal diameter and surface coating, *ACS Nano*, 2013, **7**, 9693–9703.
6 Y. Deligiannakis, G. A. Sotiriou and S. E. Pratsinis, Antioxidant and antiradical SiO_2 nanoparticles covalently functionalized with gallic acid, *ACS Appl. Mater. Interfaces*, 2012, **4**, 6609–6617.
7 C. Viglianisi, V. Di Pilla, S. Menichetti, V. M. Rotello, G. Candiani, C. Malloggi and R. Amorati, Linking an α-tocopherol derivative to cobalt(0) nanomagnets: magnetically responsive antioxidants with superior radical trapping activity and reduced cytotoxicity, *Chem. – Eur. J.*, 2014, **20**, 6857–6860.
8 B. Hu, Y. Ting, X. Zeng and Q. Huang, Bioactive peptides/chitosan nanoparticles enhance cellular antioxidant activity of (−)-epigallocatechin-3-gallate, *J. Agric. Food Chem.*, 2013, **61**, 875–881.
9 X. Xie, Q. Tao, Y. Zou, F. Zhang, M. Guo, Y. Wang, H. Wang, Q. Zhou and S. Yu, PLGA nanoparticles improve the oral bioavailability of curcumin in rats: characterizations and mechanisms, *J. Agric. Food Chem.*, 2011, **59**, 9280–9289.
10 A. Kumari, S. K. Yadav, Y. B. Pakade, B. Singh and S. C. Yadav, Development of biodegradable nanoparticles for delivery of quercetin, *Colloids Surf., B*, 2010, **80**, 184–192.
11 Y. M. Lvov, D. G. Shchukin, H. Mohwald and R. R. Price, Halloysite clay nanotubes for controlled release of protective agents, *ACS Nano*, 2008, **2**, 814–820.
12 H. Zhang, T. Ren, Y. Ji, L. Han, Y. Wu, H. Song, L. Bai and X. Ba, Selective modification of halloysite nanotubes with 1-pyrenylboronic acid: a novel fluorescence probe with highly selective and sensitive response to hyperoxide, *ACS Appl. Mater. Interfaces*, 2015, **7**, 23805–23811.
13 F. Arcudi, G. Cavallaro, G. Lazzara, M. Massaro, S. Milioto, R. Noto and S. Riela, Selective functionalization of halloysite cavity by click reaction: structured filler for enhancing mechanical properties of bionanocomposite films, *J. Phys. Chem. C*, 2014, **118**, 15095–15101.
14 G. Cavallaro, G. Lazzara, M. Massaro, S. Milioto, R. Noto, F. Parisi and S. Riela, Biocompatible poly(*N*-isopropylacrylamide)-halloysite nanotubes for thermoresponsive curcumin release, *J. Phys. Chem. C*, 2015, **119**, 8944–8951.

15 N. G. Veerabadran, D. Mongayt, V. Torchilin, R. R. Price and Y. M. Lvov, Organized shells on clay nanotubes for controlled release of macromolecules, *Macromol. Rapid Commun.*, 2009, **30**, 99–103.
16 M. Massaro, R. Amorati, G. Cavallaro, S. Guernelli, G. Lazzara, S. Milioto, R. Noto, P. Poma and S. Riela, Direct chemical grafted curcumin on halloysite nanotubes as dual-responsive prodrug for pharmacological applications, *Colloids Surf., B*, 2016, **140**, 505–513.
17 Y. Fu, D. Zhao, P. Yao, W. Wang, L. Zhang and Y. Lvov, Highly aging-resistant elastomers doped with antioxidant-loaded clay nanotubes, *ACS Appl. Mater. Interfaces*, 2015, **7**, 8156–8165.
18 S. Riela, M. Massaro, C. G. Colletti, A. Bommarito, C. Giordano, S. Milioto, R. Noto, P. Poma and G. Lazzara, Development and characterization of co-loaded curcumin/triazole-halloysite systems and evaluation of their potential anticancer activity, *Int. J. Pharm.*, 2014, **475**, 613–623.
19 M. Massaro, S. Piana, C. G. Colletti, R. Noto, S. Riela, C. Baiamonte, C. Giordano, G. Pizzolanti, G. Cavallaro, S. Milioto and G. Lazzara, Multicavity halloysite–amphiphilic cyclodextrin hybrids for co-delivery of natural drugs into thyroid cancer cells, *J. Mater. Chem. B*, 2015, **3**, 4074–4081.
20 V. Vergaro, Y. M. Lvov and S. Leporatti, Halloysite clay nanotubes for resveratrol delivery to cancer cells, *Macromol. Biosci.*, 2012, **12**, 1265–1271.
21 A. L. Chun, Will the public swallow nanofood?, *Nat. Nanotechnol.*, 2009, **4**, 790–791.
22 R. Amorati, M. C. Foti and L. Valgimigli, Antioxidant activity of essential oils, *J. Agric. Food Chem.*, 2013, **61**, 10835–10847.
23 J. A. Garde, R. Catalá, R. Gavara and R. J. Hernandez, Characterizing the migration of antioxidants from polypropylene into fatty food simulants, *Food Addit. Contam.*, 2001, **18**, 750–762.
24 E. A. Decker, K. Warner, M. P. Richards and F. Shahidi, Measuring antioxidant effectiveness in food, *J. Agric. Food Chem.*, 2005, **53**, 4303–4310.
25 J. M. Cruz, E. Conde, H. Domínguez and J. C. Parajó, Thermal stability of antioxidants obtained from wood and industrial wastes, *Food Chem.*, 2007, **100**, 1059–1064.
26 L. Valgimigli and D. A. Pratt, Maximizing the reactivity of phenolic and aminic radical-trapping antioxidants: just add nitrogen!, *Acc. Chem. Res.*, 2015, **48**, 966–975.
27 C. Queiroz, A. J. Ribeiro da Silva, M. L. Mendes Lopes, E. Fialho and V. L. Valente-Mesquita, Polyphenol oxidase activity, phenolic acid composition and browning in cashew apple (Anacardium occidentale, L.) after processing, *Food Chem.*, 2011, **125**, 128–132.
28 L. Manzocco, S. Calligaris, D. Mastrocola, M. C. Nicoli and C. R. Lerici, Review of nonenzymatic browning and antioxidant capacity in processed foods, *Trends Food Sci. Technol.*, 2001, **11**, 340–346.
29 V. Vergaro, E. Abdullayev, Y. M. Lvov, A. Zeitoun, R. Cingolani, R. Rinaldi and S. Leporatti, Cytocompatibility and uptake of halloysite clay nanotubes, *Biomacromolecules*, 2010, **11**, 820–826.
30 G. I. Fakhrullina, F. S. Akhatova, Y. M. Lvov and R. F. Fakhrullin, Toxicity of halloysite clay nanotubes *in vivo*: a caenorhabditis elegans study, *Environ. Sci.: Nano*, 2015, **2**, 54–59.
31 L. Valgimigli, M. Lucarini, G. F. Pedulli and K. U. Ingold, Does β-carotene really protect vitamin E from oxidation?, *J. Am. Chem. Soc.*, 1997, **119**, 8095–8096.
32 S. Kumar, H. Johansson, L. Engman, L. Valgimigli, R. Amorati, M. G. Fumo and G. F. Pedulli, Regenerable chain-breaking 2,3-dihydrobenzo[*b*]selenophene-5-ol antioxidants, *J. Org. Chem.*, 2007, **72**, 2583–2595.
33 L. Valgimigli, D. Bartolomei, R. Amorati, E. Haidasz, J. J. Hanthorn, S. J. Nara, J. Brinkhorst and D. A. Pratt, 3-Pyridinols and 5-pyrimidinols: tailor-made for use in synergistic radical-trapping co-antioxidant systems, *Beilstein J. Org. Chem.*, 2013, **9**, 2781–2792.
34 M. C. Foti, C. Daquino, G. A. Di Labio and K. U. Ingold, Kinetics of the oxidation of quercetin by 1,1-diphenyl-2-picrylhydrazyl (DPPH$^{\bullet}$), *Org. Lett.*, 2011, **13**, 4826–4829.
35 M. Russo, C. Spagnuolo, I. Tedesco, S. Bilotto and G. L. Russo, The flavonoid quercetin in disease prevention and therapy: facts and fancies, *Biochem. Pharmacol.*, 2012, **83**, 6–15.
36 P. Djomgoue and D. Njopwouo, FT-IR spectroscopy applied for surface clays characterization, *J. Surf. Eng. Mater. Adv. Technol.*, 2013, **3**, 275–282.
37 K. P. Nicolini, C. R. B. Fukamachi, F. Wypych and A. S. Mangrich, Dehydrated halloysite intercalated mechanochemically with urea: thermal behavior and structural aspects, *J. Colloid Interface Sci.*, 2009, **338**, 474–479.
38 É. Makó, J. Kristóf, E. Horváth and V. Vágvölgyi, Kaolinite–urea complexes obtained by mechanochemical and aqueous suspension techniques – a comparative study, *J. Colloid Interface Sci.*, 2009, **330**, 367–373.
39 L. Gastaldi, E. Ugazio, S. Sapino, P. Iliade, I. Miletto and G. Berlier, Mesoporous silica as a carrier for topical application: the Trolox case study, *Phys. Chem. Chem. Phys.*, 2012, **14**, 11318–11326.
40 M. Massaro, C. G. Colletti, R. Noto, S. Riela, P. Poma, S. Guernelli, F. Parisi, S. Milioto and G. Lazzara, Pharmaceutical properties of supramolecular assembly of co-loaded cardanol/triazole-halloysite systems, *Int. J. Pharm.*, 2015, **478**, 476–485.
41 G. Cavallaro, G. Lazzara and S. Milioto, Exploiting the colloidal stability and solubilization ability of clay nanotubes/ionic surfactant hybrid nanomaterials, *J. Phys. Chem. C*, 2012, **116**, 21932–21938.
42 P. Yuan, P. D. Southon, Z. Liu, M. E. R. Green, J. M. Hook, S. J. Antill and C. J. Keper, Functionalization of halloysite clay nanotubes by grafting with γ-aminopropyltriethoxysilane, *J. Phys. Chem. C*, 2008, **112**, 15742–15751.
43 W. Shen, H. He, J. Zhu, P. Yuan and R. L. Frost, Grafting of montmorillonite with different functional silanes via two different reaction systems, *J. Colloid Interface Sci.*, 2007, **313**, 268–273.
44 S. A. V. Eremia, D. Chevalier-Lucia, G.-L. Radu and J.-L. Marty, Optimization of hydroxyl radical formation using

TiO_2 as photocatalyst by response surface methodology, *Talanta*, 2008, **77**, 858–862.

45 R. Amorati, G. F. Pedulli and L. Valgimigli, Kinetic and thermodynamic aspects of the chain-breaking antioxidant activity of ascorbic acid derivatives in non-aqueous media, *Org. Biomol. Chem.*, 2011, **9**, 3792–3800.

46 R. Amorati, L. Valgimigli, L. Panzella, A. Napolitano and M. d'Ischia, 5-*S*-Lipoylhydroxytyrosol, a multidefense antioxidant featuring a solvent-tunable peroxyl radical-scavenging 3-thio-1,2-dihydroxybenzene motif, *J. Org. Chem.*, 2013, **78**, 9857–9864.

47 M. Musialik and G. Litwinienko, Scavenging of DPPH$^{\bullet}$ radicals by vitamin E is accelerated by its partial ionization: the role of sequential proton loss electron transfer, *Org. Lett.*, 2005, **7**, 4951–4954.

48 M. Musialik, R. Kuzmicz, T. S. Pawłowski and G. Litwinienko, Acidity of hydroxyl groups: an overlooked influence on antiradical properties of flavonoids, *J. Org. Chem.*, 2009, **74**, 2699–2709.

49 R. Amorati, P. T. Lynett, L. Valgimigli and D. A. Pratt, The reaction of sulfenic acids with peroxyl radicals: insights into the radical-trapping antioxidant activity of plant-derived thiosulfinates, *Chem. – Eur. J.*, 2012, **18**, 6370–6379.

50 P. Mendes, Biochemistry by numbers: simulation of biochemical pathways with Gepasi 3, *Trends Biochem. Sci.*, 1997, **22**, 361–363.

51 G. Cavallaro, G. Lazzara, S. Milioto, G. Palmisano and F. Parisi, Halloysite nanotube with fluorinated lumen: non-foaming nanocontainer for storage and controlled release of oxygen in aqueous media, *J. Colloid Interface Sci.*, 2014, **417**, 66–71.

52 L. Nordstierna, I. Furó and P. Stilbs, Mixed adsorption of fluorinated and hydrogenated surfactants, *Langmuir*, 2006, **22**, 7969–7974.

53 C. Aguzzi, C. Viserasa, P. Cerezo, I. Salcedo, R. Sánchez-Espejo and C. Valenzuela, Release kinetics of 5-aminosalicylic acid from halloysite, *Colloids Surf., B*, 2013, **105**, 75–80.

54 S. Kumar, H. Johansson, T. Kanda, L. Engman, T. Müller, H. Bergenudd, M. Jonsson, G. F. Pedulli, R. Amorati and L. Valgimigli, Catalytic chain-breaking pyridinol antioxidants, *J. Org. Chem.*, 2010, **75**, 716–725.

55 M. Lucarini, G. F. Pedulli, L. Valgimigli and R. Amorati, Thermochemical and kinetic studies of a bisphenol antioxidant, *J. Org. Chem.*, 2001, **66**, 5456–5462.